*M&C 2017 - International Conference on Mathematics & Computational Methods Applied to Nuclear Science & Engineering, Jeju, Korea, April 16-20, 2017, on USB (2017)*

# Extension of the Component Thermal-Hydraulics Analysis code CUPID toward Subchannel Scale Analysis of Rod Bundle Geometry under Isothermal Single and Two-phase Conditions

Seok-Jong Yoon, Goon-Cherl Park and Hyoung-Kyu Cho*

*Seoul National University, 151-744, 1 Gwanak-ro, Gwanak-gu, Seoul, Rep. of Korea*
*ysk1006@snu.ac.kr, parkgc@snu.ac.kr, chohk@snu.ac.kr**

**Abstract** - *It becomes critical issue in the nuclear reactor safety analysis that high-fidelity and multi-physics simulation with coupled T/H (Thermal-Hydraulics) and neutronics code for a full core of light water reactor under reactivity induced accident conditions. Considering the computational power necessary for a full core pin-by-pin analysis, subchannel scale analysis is desired to achieve both required accuracy and acceptable computational time. In the present study, feasibility test for the application of the KAERI's inhouse code CUPID for subchannel scale T/H analysis was carried out. The validation results of CUPID for subchannel scale analysis of rod bundle experiments under isothermal single-phase and two-phase flow conditions were introduced. Prior to the simulation, key subchannel models including pressure drop, EM and EVVD turbulent mixing models were implemented to CUPID. Form the validation results, CUPID showed its capability of reproducing key phenomena in a subchannel.*

## Ⅰ. INTRODUCTION

It becomes critical issue in the nuclear reactor safety analysis that high-fidelity and multi-physics simulation with coupled T/H (Thermal-Hydraulics) and neutronics code for a full core of light water reactor under reactivity induced accident conditions.

The methodologies of the nuclear reactor safety analysis have been developed by advancement of computing power. High performance computing power and improved numerical schemes allow the coupled multi-physics analysis and 3D full core transient calculation. Coupled 3D full core analysis can assure higher safety margin under asymmetric power distribution conditions and minimize the economic uncertainty by optimizing the fuel design and fuel cycle costs [1].

Considering the computational power necessary for a full core pin-by-pin analysis, subchannel scale analysis is desired to achieve both required accuracy and acceptable computational time. Subchannel means imaginary flow area surrounded by fuel rods. In this scale, one computing cell represents a one subchannel in a reactor core.

Recently, in the CASL (Consortium for Advanced Simulation of Light water reactors) project [2], the subchannel T/H analysis code COBRA-TF [3] has been used for high precision full core T/H analysis with coupled other multi-physics codes. Also, AREVA has developed ARCADIA code system [4] which enables the coupled full core pin-by-pin neutronics and T/H analysis.

In Korea, subchannel T/H analysis code MATRA [5], has been developed by KAERI (Korea Atomic Energy Research Institute) and widely used for various applications. The code has been used for reactor core design and evaluating DNBR margin. However, since the main purpose of the MATRA code, some features of it are not optimized for accident analyses; for example, the HEM (Homogeneous Equilibrium Model) for the two-phase flow and spatial marching numerical scheme to solve the governing equations. It is desired to employ two-fluid model for high-precision T/H simulation under considerable boiling condition. In case of using spatial marching numerical scheme, there exists limitation of solving reverse flow.

For this reason, in the present study, feasibility test for the application of CUPID [6] code for subchannel scale T/H analysis was conducted. CUPID is a component scale T/H analysis code developed by KAERI which adopts three-dimensional two-fluid model for the governing equations. The numerical solver is highly parallelized and the code performance was tested with various simulations. These features of CUPID would be advantageous to extend its applicability for a subchannel scale full core simulation of an accident condition.

In this paper, key subchannel models were implemented to CUPID. For the analysis of single-phase and two-phase flow with isothermal incompressible flow conditions, pressure drop and turbulent mixing models were implemented to CUPID with consideration of flow direction. Thereafter, the code was validated against five rod bundle flow mixing experiments. For isothermal single-phase flow, four tests including CNEN 4x4 test [7], PNL 7x7 test [8], CE 15x15 test [9], WH 14x14 test [10] were selected and the calculation results of CUPID were compared with the calculation results of MATRA and the experimental data. For isothermal two-phase flow, RPI air-water test [11] was validated.

## Ⅱ. IMPLEMENTATION OF SUBCHANNEL MODELS TO CUPID

The CUPID code adopts a transient three-dimensional two-fluid models for the governing equations. It uses porous media approach for describing flow field in the reactor core.

Geometries of fuel rods are simplified with a given porosity in control volumes as shown in Fig. 1. Convection and diffusion at each cell face are considered with permeability. Porosity and permeability are applied at the volume and surface integral by the Finite Volume Method (FVM), respectively.

The fluid transfer between adjacent subchannels can be explained by three mechanisms, i.e. diversion crossflow, turbulent mixing and void drift [12]. These mechanisms are modeled as a closure terms to solve the mass, momentum and energy conservation equations. These models are presented by Todreas and Kazimi [13] and subchannel analysis code COBRA-TF [3] and MATRA [5].

In this chapter, governing equations which use porous media and two-fluid model are presented. Also, implemented key subchannel T/H models are introduced.

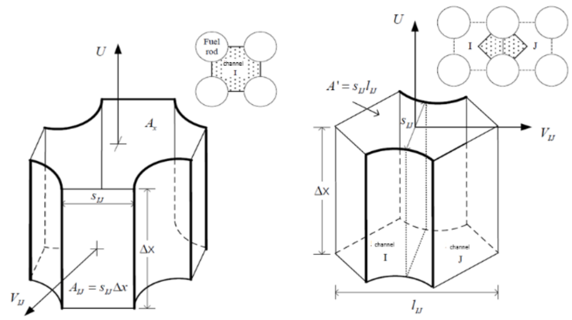


(a) Axial direction (b) Transverse direction

Fig. 1. Subchannel control volumes [5]

## 1. Governing equations

Mass conservation equation for k-field

$$\int \frac{\partial}{\partial t}\left(\alpha_k \rho_k\right) dV + \int \alpha_k \rho_k \vec{V}_k \cdot d\vec{S} = \int \Gamma_k dV + \int \vec{M}_e^T dV \quad (1)$$

Where, $\Gamma_k$ : Volumetric mass transfer rate

$\vec{M}_e^T$ : Mass exchange due to the turbulent mixing and void drift

Momentum conservation equation for k-field

$$\begin{aligned} &\int \frac{\partial}{\partial t}\left(\alpha_k \rho_k \vec{V}_k\right) dV + \int (\alpha_k \rho_k \vec{V}_k \vec{V}_k) \cdot d\vec{S} - \vec{V}_k \int (\alpha_k \rho_k \vec{V}_k) \cdot d\vec{S} \\ &= -\int \alpha_k \nabla P dV + \int \alpha_k \rho_k \vec{g} dV - \int \left(\alpha_k \mu_k \nabla \vec{V}_k\right) \cdot d\vec{S} \\ &+ \int S_k dV + \int \vec{M}_{wk} dV + \int \vec{M}_k^T dV \end{aligned} \quad (2)$$

Where, $\vec{V}_k$ : Vector velocity ( $u_k \vec{i} + v_k \vec{j} + w_k \vec{k}$ )

$S_k$ : Momentum source or sink term due to phase change

$\vec{M}_{wk}$ : Friction factor and form loss

$\vec{M}_k^T$ : Momentum transfer due to the turbulent mixing and void drift

Energy conservation equation for k-field

$$\begin{aligned} &\int \frac{\partial}{\partial t}\left(\alpha_k \rho_k e_k\right) dV + \int \left(\alpha_k \rho_k e_k \vec{V}_k\right) \cdot d\vec{S} \\ &= -\int P \frac{\partial \alpha_k}{\partial t} dV - P \int \alpha_k \vec{V}_k \cdot d\vec{S} + \int \alpha_k k_k \nabla T_k \cdot d\vec{S} + \int E_k dV \\ &+ \int \vec{M}_h^T dV + \int q''_{fluid-solid} dA + q''_{fluid-porous} A_{fluid-porous} \end{aligned} \quad (3)$$

Where, $E_k$ : Energy source or sink term due to phase change, interfacial heat transfer and volumetric heat generation

$\vec{M}_h^T$ : Energy exchange due to turbulent mixing and void drift

$q''_{fluid-porous} = h_{fluid-porous}\left(T_{porous} - T_{fluid}\right)$

$h_{fluid-porous}$ : Heat transfer coefficient between fluid and conductor in porous medium

## 2. Pressure drop model

A crossflow can occur due to the lateral pressure difference between adjacent subchannels and pressure drop model is one of the important subchannel models to analyze the fluid transfer. The pressure drop model consists of the friction factor and form loss models with consideration of flow direction. For axial direction, friction factor and grid spacer models formulated with form loss were included. These models were added as a type of pressure drop to axial momentum conservation equation as follows

$$\vec{M}_{wk} = -\frac{1}{2}\left(\frac{f}{d_{hy}} + K\right)\left(\frac{G^2}{\rho}\right)\Phi \quad (4)$$

$$f = a\,\mathrm{Re}^b + c \quad (5)$$

Where, $f$ : Wall friction factor

$d_{hy}$ : Hydraulic diameter

$\Phi$ : Two-phase multiplier

$G$ : Mass flux

$K$ : Form loss coefficient for a grid spacer

Wall friction factor is the function of Reynolds number as indicated in Eq. 5 and it is defined differently with laminar and turbulent flow condition as shown in Table 1.

Table 1. Wall friction factor coefficient [5]

| Flow condition | a | b | c | Effective Region |
|---|---|---|---|---|
| Laminar | 64.0 | -1.0 | 0.0 | Re<2,300 |
| Turbulent (Blasius type) | 0.32 | 0.25 | 0.0 | 2,300<Re<30,000 |
| Turbulent (McAdams type) | 0.18 | 0.20 | 0.0 | $3\times10^4$<Re<$10^6$ |

For considering the additional pressure drop at two-phase flow, two-phase multiplier which is proposed by Armand [14] is applied. Two-phase multiplier is defined using void fraction and quality as follows

$$\Phi = \frac{(1-x)^2}{(1-\alpha)^{1.42}}, \qquad 0 < \alpha \le 0.6 \tag{6}$$

$$\Phi = 0.478\frac{(1-x)^2}{(1-\alpha)^{2.2}}, \qquad 0.6 < \alpha \le 0.9 \tag{7}$$

$$\Phi = 1.73\frac{(1-x)^2}{(1-\alpha)^{1.64}}, \qquad 0.9 < \alpha < 1.0 \tag{8}$$

Considering the consecutive fuel gap change by the rod arrangement, form loss model was added to transverse momentum equation as follows

$$\vec{M}_{wk,L} = -\frac{K_G}{2}\left(\frac{W_{IJ}\left|W_{IJ}\right|}{l_{IJ}\rho_{IJ}s_{IJ}}\right) \tag{9}$$

Where, $W_{IJ} = \sum_k \alpha_k \rho_k V_{IJ,k} \times s_{IJ}$ , Mass flow which flows subchannel *I* to *J*.

$l_{IJ}$ : Length between the center of subchannel *I* and *J*

$s_{IJ}$ : Gap size between two fuel rods

$K_G$ : Transverse form loss coefficient, default value is 0.5

## 3. Turbulent Mixing Model (EM model - Equal Mass Exchange Model)

The fluid exchange can be caused by turbulent mixing due to the turbulent fluctuation and flow distribution by structures such as the grid spacer. In single-phase flow with isothermal incompressible flow condition, no net mass exchange occurs between adjacent subchannels, but both momentum and energy can be distributed by exchanging equal mass flow rates. This mechanism is modeled as EM (Equal Mass exchange) model and the model was added to momentum conservation equation as presented in Eq. 10.

$$\vec{M}_k^T = -\sum w'_{IJ}\left(V_I - V_J\right) \tag{10}$$

$$w'_{IJ} = \beta \times s_{IJ} \times \bar{G} \tag{11}$$

Where, $w'_{IJ}$ : Amount of flow mixing between subchannel *I* and *J*

$\beta$ : Turbulent mixing coefficient

$\bar{G}$ : Area-averaged axial mass flux

The turbulent mixing coefficient is determined by experimental results.

## 4. Turbulent Mixing Model (EVVD model - Equal Volume Exchange and Void Drift model)

In the case of two-phase flow or heated condition, net mass, momentum and energy exchange occurs between adjacent subchannels. This flow mechanism is modeled as EVVD (Equal Volume exchange and Void Drift) model. The turbulent mixing terms are modeled by simple diffusion approximation using mixing length theory. The EVVD model was implemented to mass, momentum and energy conservation equations as a source term presented in Eq. 12 to Eq. 14.

The turbulent mixing and void drift of mass transfer

$$\vec{M}_e^T = \varepsilon\frac{s_{IJ}}{z_{IJ}^T}\left(\rho_f - \rho_g\right)\theta\left[\alpha_{v,J} - \alpha_{v,I} - \left(\alpha_{v,J} - \alpha_{v,I}\right)_{equil}\right] \tag{12}$$

The turbulent mixing and void drift of momentum transfer

$$\vec{M}_k^T = \varepsilon\frac{s_{IJ}}{z_{IJ}^T}\left(\rho_f v_f - \rho_g v_g\right)\theta\left[\alpha_{v,J} - \alpha_{v,I} - \left(\alpha_{v,J} - \alpha_{v,I}\right)_{equil}\right] \tag{13}$$

The turbulent mixing and void drift of energy transfer

$$\vec{M}_h^T = \varepsilon\frac{s_{IJ}}{z_{IJ}^T}\left(\rho_f h_f - \rho_g h_g\right)\theta\left[\alpha_{v,J} - \alpha_{v,I} - \left(\alpha_{v,J} - \alpha_{v,I}\right)_{equil}\right] \tag{14}$$

Where, $\varepsilon$ : Eddy diffusivity

$z_{IJ}^T$ : Turbulent mixing length

$\alpha$ : Void fraction

$h$ : Enthalpy

$\theta$ : Two-phase multiplier

The first term in the square brackets indicates the equal volume exchange turbulent mixing model. Following this model, the difference of void fraction between adjacent subchannels acts driving force to derive the liquid mass to the higher void fraction and the vapor mass to the lower void subchannel. But in void drift model, vapor and liquid movements are determined to reach the equilibrium void distribution. The equilibrium void distribution was derived by Lahey [15] using mass flux difference between adjacent subchannels as presented in Eq. 15. This effect is captured with the second term in the square brackets.

$$\left(\alpha_{v,I} - \alpha_{v,J}\right)_{equil} = K_a \left(\alpha_{v,I} + \alpha_{v,J}\right) \frac{G_I - G_J}{G_I + G_J} \tag{15}$$

Scaling factor $K_a$ is generally taken to be 1.4. The mixing term is defined using the turbulent mixing coefficient and area-averaged axial mass flux and density as shown in Eq. 16.

$$\varepsilon \frac{s_{IJ}}{z_{IJ}^{T}} = \frac{\beta \bar{G} s_{IJ}}{\bar{\rho}} \tag{16}$$

Turbulent mixing coefficient is defined as a ratio of the transverse mass flux to the axial mass flux. But, in most cases turbulent mixing coefficient is defined by users' input.

The two-phase multiplier in EVVD model was proposed by Beus [16] as follows,

$$\theta = 1 + \left(\theta_M - 1\right)\left(\frac{x}{x_M}\right) \qquad x < x_M \tag{17}$$

$$\theta = 1 + \left(\theta_M - 1\right)\left(\frac{x_M - x_0}{x - x_0}\right) \qquad x > x_M \tag{18}$$

Where, $x$ : Quality

$\theta_M$ : Two phase mixing coefficient at the transition point (given 5 by Faya)

$x_M$ : Quality at the slug-annular transition point

$x_0 / x_M = 0.75\,\mathrm{Re}^{0.0417}$

Quality at the slug-annular transition point is defined using Wallis model [17] as shown in Eq. 19.

$$x_M = \frac{\dfrac{0.4\left[\rho_f\left(\rho_f - \rho_g\right) g D_h\right]^{1/2}}{G} + 0.6}{\left(\dfrac{\rho_f}{\rho_g}\right)^{1/2} + 0.6} \tag{19}$$

**5. Constitutive models for two-phase flow analysis in CUPID**

For analyzing two-phase flow conditions, CUPID-SG (CUPID code for Steam Generators) subroutine [18] was already built in CUPID. It has various constitutive models for two-phase flow analysis including flow regime map, interfacial area concentration, interfacial momentum transfer, interfacial heat and mass transfer and heat partitioning, etc. For two-phase flow analysis in rod bundle, CUPID-SG subroutine was activated in the simulation.

## Ⅲ. VALIDATION RESULTS OF CUPID

For the code validation, four isothermal single-phase flow and one isothermal two-phase flow experiments were selected and the calculation results of CUPID were compared with the calculation results of MATRA, CTF and available experimental data.

**Validation against isothermal single-phase flow**

Four isothermal single-phase flow experiments include CNEN 4x4 [7] test for verifying mixing effect between adjacent subchannels, PNL 7x7 [8] flow blockage test for verifying velocity redistribution near blockage, CE 15x15 [9] inlet jetting test for verifying the effect of non-uniform inlet velocity to flow redistribution in the rod bundle and WH 14x14 [10] blockage test for investigating flow distribution between two open 14x14 rod bundles when partial or complete blockage occurs at the entrance of one assembly were selected.

In CNEN 4x4 test, liquid velocity was measured at the outlet of corner, side and center subchannels under various inlet liquid velocity conditions. The test section includes a bundle of 16 unheated rods of 0.015 m diameter, 0.019 m pitch and the assembly width is 0.08 m, height is 1.4 m. One grid spacer was located at the middle elevation of rod bundle. The cross sectional view of test section is shown in Fig. 2.

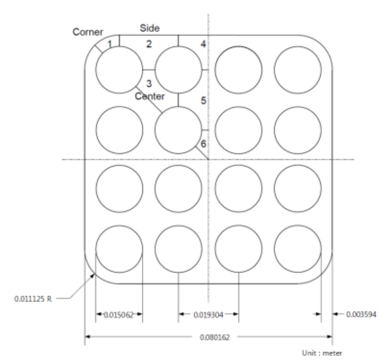


Fig. 2. Cross sectional view of CNEN test section

With applying the grid spacer model, CUPID could calculate the pressure drop along the axial direction and the result was agreed with the calculation results of MATRA as shown in Fig. 3. Fig. 4 shows the three-dimensional calculation result of liquid velocity contour at eight different axial elevations. The liquid is concentrated to the center subchannels as it flows upward. This occurs due to the pressure drop model which attributes low flow resistance at center subchannels compared to others.

Also, calculations for verifying the effect of EM model were performed. Without applying the EM model, the momentum loss at the corner and side subchannels cannot be compensated and outlet liquid velocities were underestimated. But, in the case of applying EM model, CUPID could properly capture the experimental data within the error range of -2.6 ~ 0.5 % at the corner and -1.8 ~ 0.8 % at the center as shown in Fig. 5.

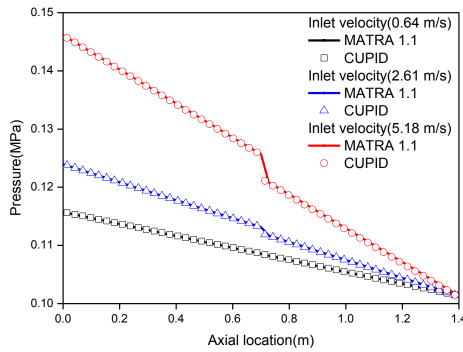


Fig. 3. Pressure drop along axial direction

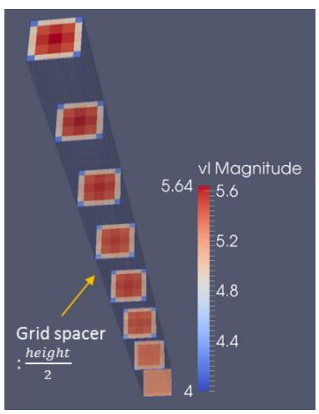


Fig. 4. Velocity contour along axial elevation

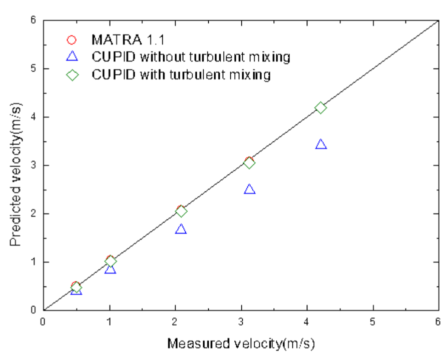


(a) Outlet velocity at corner subchannel

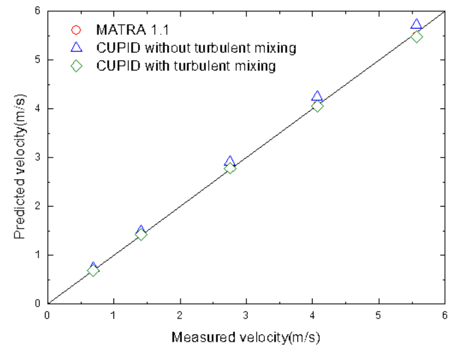


(b) Outlet velocity at center subchannel

Fig. 5. Outlet velocity at corner and center subchannels

The PNL 7x7 test simulated the flow blockage phenomena during the Loss-Of-Coolant Accident (LOCA) at pressurized water reactors. The postulated sleeve blockage at the nine central rods in the bundle was adopted for describing 70 % area reduction in the four central subchannels between two grid spacers. The change of subchannel geometry near the blockage rods were considered in the calculation as summarized in Table 2. The test section consists of 7x7 rod array of 0.01 m diameter pins with pitches of 0.0137 m and the width of assembly is 0.1033 m. Three grid spacers were positioned in rod bundle. The test was performed at 0.12 MPa, 302.6 K and inlet Reynolds number, $2.95{\times}10^4$. The cross sectional and longitudinal view of test section were depicted in Fig. 6.

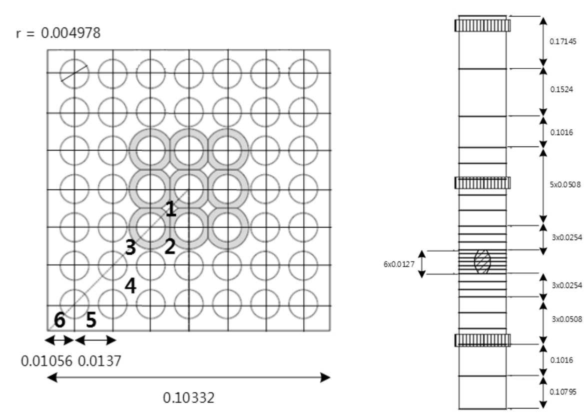


Fig. 6. Features of PNL 7x7 test sections

Table 2. Subchannel geometry change near blockage

| Subchannel number | Porosity | Hydraulic diameter(m) |
|---|---|---|
| 1 | 0.1756 | 0.0043 |
| 2 | 0.3778 | 0.0083 |
| 3 | 0.4805 | 0.0104 |

| | | |
|---|---|---|
| 4 | 0.5852 | 0.0140 |
| 5 | 0.7309 | 0.0144 |
| 6 | 0.8255 | 0.0127 |

The phenomenon including bypass flow in front of the blockage, jet effect at the blockage and flow recovery by turbulent mixing after passage of the blockage were reasonably reproduced by CUPID as shown in Fig. 7.

Further calculation was carried out with increasing blockage ratio up to 99 %. In this problem case, lateral flows are dominant so there may exist limitation in solving with the spatial marching numerical scheme. However, CUPID adopts pressure velocity linked scheme to solve the governing equations and solves the momentum conservation equations for whole computational domain at once by building a system of the pressure correction equations. With increasing blockage ratio, the amount of liquid flows in to the channel 1 decreases and significantly reduced flow rate in the subchannel was qualitatively well calculated without calculation instability as shown in Fig. 8.

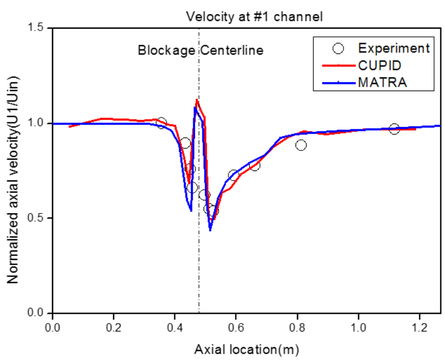


Fig. 7. Velocity along axial line at channel 1

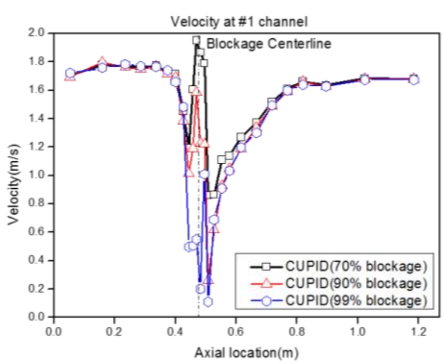


Fig. 8. Velocity with increasing blockage ratio

The objective of CE 15x15 test was for verifying the influence of non-uniform inlet velocity to flow distribution in rod bundle. The test section consists of 225 unheated rods of 0.0159 m diameter, 0.0213 m pitch, and the assembly width and height are 0.3259 m and 1.1684 m, respectively. One grid spacer was located at the middle of assembly. The cross sectional and longitudinal view of test section were depicted in Fig. 9.

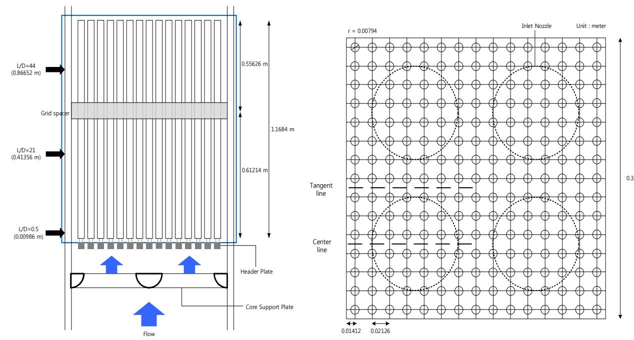


Fig. 9. Features of CE 15x15 test sections

The test was conducted at atmospheric pressure and room temperature conditions. The local liquid velocity was measured by pitot tube traversing tangent line and center line at three different axial elevations ($L/D_e = 0.5, 21, 44$). The calculation results of CUPID were compared to the calculation results of MATRA and the experimental data as shown in Fig. 10. With the effect of pressure drop and EM model, non-uniform velocity distributions go to uniform velocity distributions as flows upward. The maximum error of CUPID at center line is 8.2 % and tangent line is 9 % with compared to the experimental data.

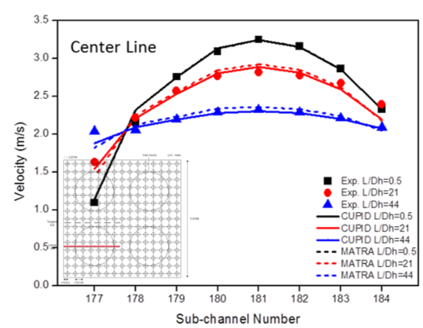


(a) Velocity at center line

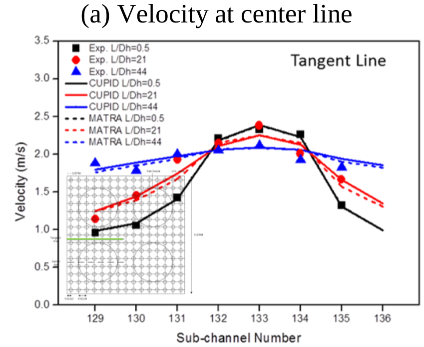


(b) Velocity at tangent line

Fig. 10. Velocity traversing at center and tangent line

The WH 14x14 test investigated the flow redistribution between two open 14x14 fuel assemblies caused by partial or complete blockage which can occur at the entrance of one assembly. Inlet mass flows were set different at two fuel assemblies to simulate a partially or completely blocked in one of the assemblies. The test section consists of two open 14x14 assemblies with a rod diameter 0.0108 m, a pitch to diameter (pitch/diameter) 1.28 and two assemblies are connected with water gap. The cross sectional view of test section was presented in Fig. 11.

The test was conducted at atmospheric pressure 0.1 MPa, and room temperature 299.8 K. In the case of partial blockage, inlet liquid velocities at bundle 1, bundle 2 and water gap were set 3.52 m/s, 1.76 m/s and 2.64 m/s, respectively.

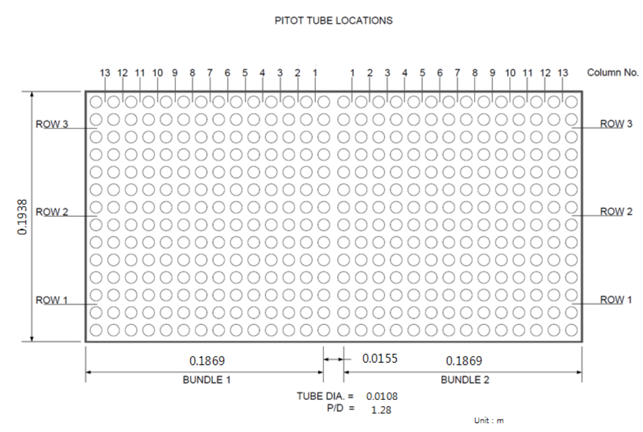


Fig. 11. Cross sectional view of WH 14x14 test section

Following the calculation results, mass flows in each bundle are gradually flattened as the liquid flows upward. Fig. 12 shows the percent of total flow at bundle 1 and bundle 2 along axial locations, and it indicates that flow mixing occurs between two assemblies.

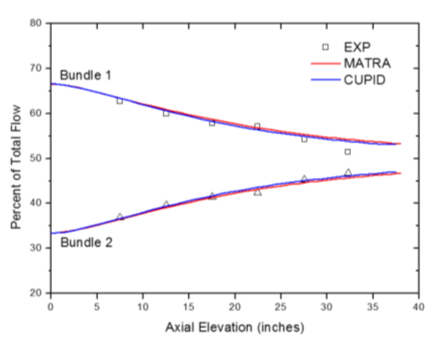


Fig. 12. Percent of total flow at bundle 1 and bundle 2

Additionally, the case of complete blockage was simulated to confirm the blockage modeling capability of CUPID. In this case, inlet liquid velocity at bundle 2 was set 0. Qualitatively reasonable calculation result was obtained including the flow recirculation near the entrance of the completely blocked assembly as shown in Fig. 13. From these analysis, CUPID showed its capability of handling reverse flow.

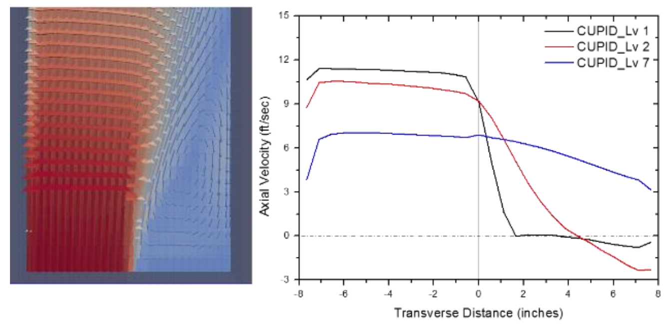


Fig. 13. Flow recirculation at complete blockage case

**Validation against isothermal two-phase flow**

For the code validation against isothermal two-phase flow, RPI air-water test which investigated the fully developed two-phase flow distributions at the exit of each subchannels was selected. In the test, void fraction was measured at the outlet of corner, side and center subchannels under various flow regime conditions, bubbly, slug and churn turbulent flow. The test section includes a bundle of 2x2 unheated rods of 0.025 m diameter, 0.035 m pitch and the width of assembly is 0.076 m, height is 0.914 m.

For verifying the effect of the EVVD model, calculated void fraction results at the outlet of each subchannels with applying the model or not are compared in Fig. 14. With the effect of the EVVD model, voids concentrated to the center subchannel as flows upward. The calculation results of CUPID with applying the EVVD model could capture the experimental data around 10 % error and show same trend with the calculation results of CTF as shown in Fig. 15.

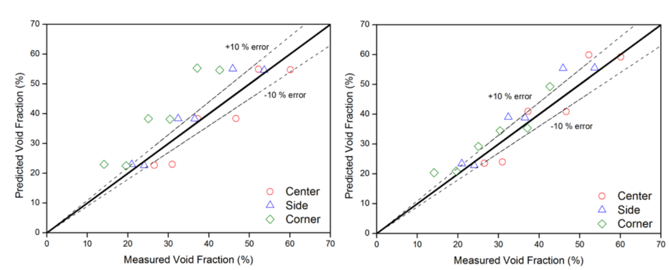


(a) Without EVVD model (b) With EVVD model

Fig. 14. Void fraction at the outlet of subchannels

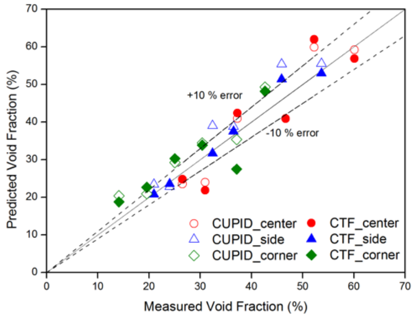


Fig. 15. Void fraction results compared with CTF results

## Ⅳ. CONCLUSIONS

In this study, the validation results of CUPID for subchannel scale analysis of rod bundle geometry under isothermal single-phase and two-phase flow conditions were introduced. Prior to the simulation, key subchannel models were implemented to CUPID. The pressure drop model was added as a viscous shear stress term in momentum conservation equations with consideration of flow direction. Also, EM turbulent mixing model was implemented for analyzing of isothermal single-phase flow condition. However, in the case of two-phase flow condition, EVVD turbulent mixing model was implemented.

Afterwards, the code was validated against isothermal single-phase and two-phase flow subchannel experiments. From these validation results, CUPID showed its capability of reproducing key phenomena in a subchannel. In addition, it was revealed that CUPID could handle a reverse flow which cannot be reproduced with spatial marching numerical scheme.

In the future, the scope of validation will be extended and required models will be improved or implemented to CUPID.

## ACKNOWLEDGMENTS

This work was supported by National R&D program through the Ministry of Education of the Republic of Korea and National Research Foundation of Korea (NRF). (No. NRF-2015M2A8A4021769)

## REFERENCES

1. G. Albin, et al., "LWR Core Safety Analysis with Areva's 3-dimensional Methods", International Journal for Nuclear Power, 58, pp. 82-87 (2013).
2. T. S. Blyth, "Improvement of COBRA-TF Subchannel Thermal-Hydraulics Code (CTF) using Computational Fluid Dynamics", CASL Technical Report, CASL-U-2015-0020-000 (2015).
3. R. Salko and M. Avramova, "CTF Theory Manual", Pennsylvania State University (2014).
4. AREVA, "The ARCADIA Reactor Analysis System for PWRs Methodology Description and Benchmarking Results", ANP-10297NP, AREVA NP Inc (2010).
5. D. H. Hwang, et al., "Validation of a Subchannel Analysis Code MATRA Version 1.0", KAERI/TR-3639/2008, KAERI (2008).
6. Korea Atomic Energy Research Institute, "CUPID Code Manuals Vol. 1: Mathematical Models and Solution Methods Version 1.9" (2014).
7. V. Marinelli, et al., "Experimental Investigation of Mass Velocity Distribution and Velocity Profiles in an LWR Rod Bundle", Trans. ANS 15, pp 413-415 (1972).
8. J. M. Creer, et al., "Effects of Sleeve Blockages on Axial Velocity and Intensity of Turbulence in an Unheated 7x7 Rod Bundle", Pacific Northwest Laboratories, BNWL-1965 (1976).
9. R. C. Marshall, et al., "Influence of Inlet Geometry on Flow in the Entrance Region of a Nuclear Reactor Rod Bundle", ASME, 68-WA/HT-34, pp.1-8 (1969).
10. H. Chelemer, et al., "THINC-IV: an Improved Program for Thermal-Hydraulic Analysis of Rod Bundle Cores", WCAP-7956, Westinghouse Electric Corp. (1973).
11. R. W. Sterner, et al., "Air-Water Subchannel Measurements of the Equilibrium Quality and Mass Flux Distribution in a Rod Bundle", NUREG/CR-3373 (1983).
12. R. T. Lahey, et al., *The thermal hydraulics of boiling water nuclear reactor*, 2nd edition, American Nuclear Society, La Grange Park (1993).
13. N. E. Todreas, et al., *Nuclear Systems Ⅱ, Elements of Thermal Hydraulic Design*, chap 6, Taylor & Francis (1990).
14. A. A. Armand, "The Resistance During the Movement of a Two-phase System in Horizontal Pipes", translated by V. Beak, AERE Trans 828 (1946).
15. R. T. Lahey and F. J. Moody, "The Thermal-Hydraulics of a Boiling Water Nuclear Reactor", Technical report, ANS Monograph (1977).
16. S. G. Beus, "A Two-Phase Turbulent Mixing Model for Flow in Rod Bundles", Technical Report WAPD-TM-2438, Bettis Atomic Power Laboratory (1971).
17. G. B. Wallis, *One-Dimensional Two-Phase Flow*, McGraw-Hill (1969).
18. H. R. Kim, et al., "Development of CUPID-SG for the analysis of two-phase flows in PWR steam generators", Progress in Nuclear Energy, Vol. 77, pp. 132-140 (2014).